Trading sensitivity for information: Carr–Purcell–Meiboom–Gill acquisition in solid-state NMR

Krishna K. Dey, Jason T. Ash, Nicole M. Trease, and Philip J. Grandinetti[a)]
Department of Chemistry, Ohio State University, 100 West 18th Avenue, Columbus, Ohio 43210, USA

(Received 22 March 2010; accepted 23 June 2010; published online 2 August 2010)

The Carr–Purcell–Meiboom–Gill (CPMG) experiment has gained popularity in solid-state NMR as a method for enhancing sensitivity for anisotropically broadened spectra of both spin 1/2 and half integer quadrupolar nuclei. Most commonly, the train of CPMG echoes is Fourier transformed directly, which causes the NMR powder pattern to break up into a series of sidebands, sometimes called "spikelets." Larger sensitivity enhancements are observed as the delay between the π pulses is shortened. As the duration between the π pulses is shortened, however, the echoes become truncated and information about the nuclear spin interactions is lost. We explored the relationship between enhanced sensitivity and loss of information as a function of the product $\Omega\ 2\tau$, where Ω is the span of the anisotropic lineshape and 2τ is the π pulse spacing. For a lineshape dominated by the nuclear shielding anisotropy, we found that the minimum uncertainty in the tensor values is obtained using $\Omega\ 2\tau$ values in the range $\Omega\ 2\tau \approx 12^{+6}_{-1}$ and $\Omega\ 2\tau \approx 9^{+3}_{-3}$ for $\eta_s=0$ and $\eta_s=1$, respectively. For an anisotropic second-order quadrupolar central transition lineshape under magic-angle spinning (MAS), the optimum range of $\Omega\ 2\tau \approx 9^{+3}_{-2}$ was found. Additionally, we show how the Two-dimensional One Pulse (TOP) like processing approach can be used to eliminate the cumbersome sideband pattern lineshape and recover a more familiar lineshape that is easily analyzed with conventional lineshape simulation algorithms.
 [doi:10.1063/1.3463653]

I. INTRODUCTION

In spite of modern hardware and improved methodologies, the lack of sensitivity in solid-state NMR spectroscopy still remains an obstacle to greater widespread adoption. While anisotropic nuclear spin interactions provide a wealth of structural information in solid-state NMR, these same interactions are also responsible for inhomogeneously broadened resonances that cause notoriously low signal-to-noise ratios. Solid-state NMR experiments, such as magic-angle spinning (MAS), manipulate the sample's spatial degrees of freedom to refocus the time-domain evolution into a train of rotary echoes. The increase in signal area in the time-domain from the multiple echoes leads to a corresponding increase in signal intensity in the frequency domain. A similar effect can be obtained using the Carr–Purcell–Meiboom–Gill (CPMG) experiment[1,2] where a train of π pulses, which manipulate the spin degrees of freedom, create a train of Hahn spin echoes.[3] Although the CPMG experiment was originally developed for diffusion and relaxation studies in liquid-state NMR, its ability to refocus spin degrees of freedom that are odd order in $\hat{I}_z$ has made it a popular approach for enhancing solid-state NMR sensitivity of anisotropic spectra for both spin-1/2 and the central transition (CT) of half integer quadrupolar nuclei in polycrystalline samples.[4–6]

While shorter delays between π pulses in the CPMG experiment can provide higher sensitivity for anisotropic spectra, it also results a corresponding information loss about anisotropic interactions, such as the chemical shift anisotropy (CSA) and quadrupolar couplings. In contrast, longer delays between π pulses retain anisotropic coupling information, but the cost is a spectrum with a lower overall sensitivity. This issue has been examined by Lefort *et al.*[7] in the context of CPMG acquisition and the multiple-quantum MAS experiment. In the Lefort study, the optimum range of CPMG π pulse spacings was defined only in terms of minimizing the truncation of the echo signal decay. As shown by Hodgkinson and Emsley[8] in the analogous case of MAS sideband analysis, however, a more appropriate merit function is the uncertainty in the tensor parameters obtained from a least-squares analysis of the sideband (or "spikelet") pattern. In this work, we have extended the approach of Hodgkinson and Emsley to the case of CPMG acquisition and found that there exists a range of optimum π pulse spacings in the CPMG experiment which yield a minimum uncertainty when extracting the NMR tensor parameters from an anisotropic lineshape. These uncertainties can be strongly dependent on the CPMG π pulse spacing, increasing steeply at short CPMG π pulse spacings and increasing at long spacings particularly when the pre-CPMG signal sensitivity is poor. We have found that the optimum π pulse spacing depends primarily on the span of the anisotropic lineshape, Ω, and generally occurs in a range of values asymmetrically spaced around $\Omega\ 2\tau \sim 11$, regardless of the interactions contributing to the lineshape. We have also found that as the pre-CPMG sensitivity decreases, the most optimum π pulse spacing remains the same while the range of optimum $\Omega\ 2\tau$ values contracts toward the most optimum value.

[a)]URL: http://www.grandinetti.org. Electronic mail: grandinetti.1@osu.edu.

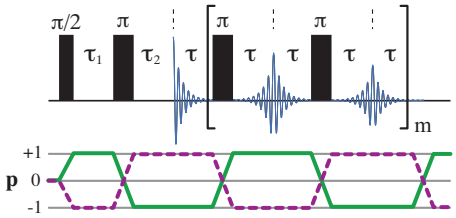

FIG. 1. CPMG pulse sequence and coherence transfer pathway used in this study.

Additionally, we demonstrate how Two-dimensional One Pulse (TOP) like processing[9–11] can also be used to eliminate the sideband (or spikelet) pattern lineshape and recover a more familiar lineshape that is easily analyzed with conventional lineshape simulation algorithms.

II. EXPERIMENTAL

All experiments were performed on a 9.4 T Bruker DMX 400 spectrometer, using a 4 mm MAS probe operating at a ^{207}Pb frequency of 83.51 MHz for polycrystalline $Pb(NO_3)_2$ and a ^{87}Rb frequency of 131.07 MHz for polycrystalline $RbClO_4$. The CPMG pulse sequence employed is shown in Fig. 1. For CPMG-MAS experiments, the π pulses were separated in time by an integer multiple of the rotor period, which was 80 μs in all experiments employing sample rotation. Radio frequency power levels were calibrated on the solution of $Pb(NO_3)_2$ and RbCl powder for ^{207}Pb and ^{87}Rb, respectively. A 1*M* $Pb(NO_3)_2$ solution and 1*M* $RbNO_3$ solution were used for referencing ^{207}Pb and ^{87}Rb resonances, respectively.

In the discussion that follows we employ IUPAC definitions for the nuclear shielding or chemical shift interaction.[12] The isotropic nuclear shielding is defined as the trace of the shielding tensor,

$$\sigma_{\mathrm{iso}} = \tfrac{1}{3}(\sigma_{xx} + \sigma_{yy} + \sigma_{zz}), \tag{1}$$

where σ_{xx}, σ_{yy}, and σ_{zz} are the components of the nuclear shielding tensor in its principal axis system. The isotropic chemical shift δ_{iso} is defined as

$$\delta_{\mathrm{iso}} = (\sigma_{\mathrm{ref}} - \sigma_{\mathrm{iso}})/(1 - \sigma_{\mathrm{ref}}), \tag{2}$$

where σ_{ref} is the isotropic nuclear shielding of a reference compound. We adopt the Haeberlen convention,[12] where

$$|\sigma_{zz} - \sigma_{\mathrm{iso}}| > |\sigma_{yy} - \sigma_{\mathrm{iso}}| > |\sigma_{xx} - \sigma_{\mathrm{iso}}|, \tag{3}$$

the shielding anisotropy ζ_s is defined as

$$\zeta_s = \sigma_{zz} - \sigma_{\mathrm{iso}}, \tag{4}$$

and the shielding asymmetry parameter is defined as

$$\eta_s = \frac{\sigma_{yy} - \sigma_{xx}}{\zeta_s}. \tag{5}$$

The components of the chemical shift tensor, δ_{ij}, are related to the components of the nuclear shielding according to

$$\delta_{ij} = (\sigma_{\mathrm{ref}} - \sigma_{ij})/(1 - \sigma_{\mathrm{ref}}), \tag{6}$$

with δ_{33} associated with the lineshape singularity furthest from δ_{iso}, and the principal component δ_{11} associated with the singularity furthest from δ_{33}, and the principal component δ_{22} associated with the singularity in between δ_{33} and δ_{11}.

A. Span

We find it convenient to define the optimum CPMG π pulse spacing in terms of the span of the anisotropic lineshape, which is defined as the difference between the maximum and minimum frequencies in the lineshape. For a nuclear shielding or chemical shift anisotropic lineshape, the span Ω_s is defined as

$$\Omega_s = \delta_{33} - \delta_{11} = -\zeta_s(\eta_s + 3)/2. \tag{7}$$

The central transition MAS spectrum of a half-integer quadrupole nucleus of spin I with an anisotropic second-order lineshape will have a span[13] of

$$\Omega_{q,\mathrm{MAS}} = \frac{\nu_q^2}{168\nu_0}\left[I(I+1) - \frac{3}{4}\right]\left(12 + 4\eta_q + \frac{\eta_q^2}{3}\right), \tag{8}$$

where ν_0 is the Larmor frequency, η_q is the quadrupole coupling asymmetry parameter, and ν_q is the quadrupole coupling splitting, given by

$$\nu_q = \frac{3C_q}{2I(2I-1)}, \tag{9}$$

with C_q as the quadrupole coupling constant.

The central transition static spectrum of a half-integer quadrupole nucleus will have an anisotropic second-order lineshape with a span[13] of

$$\Omega_{q,\mathrm{Static}} = \frac{\nu_q^2}{16\nu_0}\left[I(I+1) - \frac{3}{4}\right]\left(\frac{25}{9} + \frac{22\eta_q}{9} + \frac{\eta_q^2}{9}\right). \tag{10}$$

III. TOP PROCESSING FOR CPMG DATA

As shown by Larsen *et al.*,[4] the Fourier transform of the CPMG echo train yields a sideband or spikelet pattern. The information about unrefocused interactions is present in the individual sideband lineshape, while information about all interactions resides in the sideband envelope pattern. A problem with the sideband pattern is that any truncation artifacts in the spectrum are not easily discernable. Here we show that a TOP-like approach[11] applied to CPMG data can eliminate the sideband pattern and recover a more familiar lineshape that is easily analyzed with conventional lineshape simulation algorithms.

The decay of a CPMG echo train will arise from homogeneous interactions in addition to any motional processes which interfere with the echo refocusing. Thus, one can write the CPMG time-domain signal of a single site as

$$S(t) = s^{\mathrm{e}}(t)\sum_{N=-\infty}^{\infty} A(N)e^{i2\pi Nt/2\tau}, \tag{11}$$

where 2τ is the distance between the center of the two π pulses, $s^{\mathrm{e}}(t)$ represents the envelope function due to the unrefocused spin interactions and is responsible for the individual sideband lineshape, and $A(N)$ is the amplitude of its

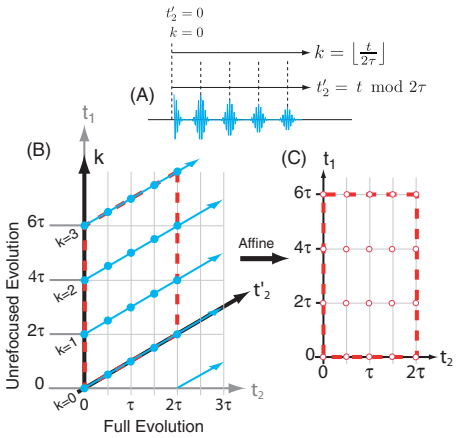

FIG. 2. (a) CPMG echoes with coordinate definitions and timings. (b) Sampling trajectory (blue lines) of the CMPG data in the 2D t_1-t_2 and $k-t_2'$ coordinate systems. Identical data sets run parallel in the 2D plane and are separated by 2τ in t_1-t_2 coordinate system. (c) Affine transformed 2D data set that correlates t_1 and t_2.

Nth sideband, which, as shown in Appendices A and B, is given by

$$A(N) = \int_0^{2\tau} e^{-iW(\alpha,\beta,\gamma)(\tau-|t-\tau|)} e^{-i2\pi Nt/2\tau} dt, \tag{12}$$

where $W(\alpha,\beta,\gamma)$ is the frequency of a crystallite at Euler angles α, β, and γ between the interaction tensor and the crystal coordinate frame.

Following the approach outlined for rotary echoes,[11] the 1D time-domain signal can be mapped into an intermediate 2D coordinate system with variables k and t_2', as shown in Fig. 2, by defining

$$t = t_2' + k2\tau, \tag{13}$$

where

$$t_2' = t \bmod 2\tau \tag{14}$$

and k is an integer given by

$$k = \left\lfloor \frac{t}{2\tau} \right\rfloor. \tag{15}$$

Here $\lfloor x \rfloor$ represents the floor function of x. Using these definitions the 1D CPMG signal can be mapped into the 2D signal in the $k-t_2'$ coordinate system obtaining

$$S(k,t_2') = s^e(k,t_2') \sum_{N=-\infty}^{\infty} A(N) e^{i2\pi Nt_2'/2\tau}.$$

To this signal we apply the affine transformation

$$\begin{pmatrix} t_1 \\ t_2 \end{pmatrix} = \begin{pmatrix} 2\tau & 1 \\ 0 & 1 \end{pmatrix} \begin{pmatrix} k \\ t_2' \end{pmatrix} \tag{16}$$

and obtain the 2D signal

$$S(t_1,t_2) = s^e(t_1,t_2) \sum_{N=-\infty}^{\infty} A(N) e^{i2\pi Nt_2/2\tau}. \tag{17}$$

A 2D Fourier transform of this signal yields a TOP-CPMG 2D spectrum, as shown in Fig. 3, which correlates interactions unrefocused by the π pulse train to all interactions. The $\omega_1=0$ cross section of the TOP-CPMG spectrum yields the TOP-CPMG-enhanced 1D spectrum.

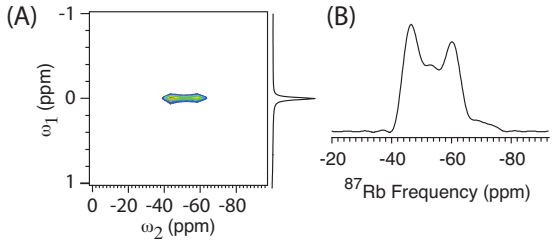

FIG. 3. (a) ^{87}Rb TOP-CPMG MAS spectrum of $RbClO_4$. The ω_1 dimension contains all the unrefocused frequencies and the ω_2 dimension contains all frequencies. The contour level for the 2D contour plot is 20%–100% with a linear increment of 4.2% of the maximum amplitude. (b) The CPMG-enhanced 1D spectrum obtained from the $\omega_1=0$ cross-section.

It is well known that the sensitivity of a spectrum will decrease with increasing acquisition time, unless a proper time-domain matched filter is applied prior to Fourier transform. Similarly, if no apodization is applied to the CPMG data before processing, the sensitivity of the sideband or TOP-CPMG spectrum will become dependent on the total CPMG acquisition time. For a CPMG signal the appropriate matched filter is one that matches the envelope function,[14] $s^e(t)$, due to the unrefocused spin interactions. The parameters for this envelope function are easily obtained from the lineshape of an individual sideband or, alternatively, the lineshape in the ω_1 projection of the TOP-CPMG 2D spectrum.

IV. RESULTS AND DISCUSSION

A. First-order chemical shift

Using TOP processed CPMG spectra, we have explored the relationship between the CPMG π pulse spacing and the tensor parameter uncertainties extracted from the CPMG-enhanced anisotropic lineshape. This idea is similar to that of Hodgkinson and Emsley,[8] who investigated the optimum spinning speed for extracting nuclear shielding anisotropy parameters in a spinning sideband analysis. They found that the minimum uncertainty in extracting the shielding anisotropy ζ_s occurred when $|\zeta_s|\tau_R \approx 9$, where τ_R is the rotor period. For the shielding asymmetry parameter η_s, they state "that static spectra always provide a more reliable determination." We believe, however, that this conclusion may have been incorrectly biased by examining reliability instead of standard deviation, since reliability in the case of η_s becomes ill-defined as η_s goes to zero.

A notable difference between CPMG and MAS is that CPMG refocuses both isotropic and anisotropic frequencies, whereas MAS refocuses only anisotropic frequencies. Thus, with increasing MAS speed or decreasing CPMG π pulse spacing the uncertainty in nuclear shielding anisotropy parameters, ζ_s and η_s, increases in both methods. In contrast, the uncertainty in the isotropic chemical shift decreases in MAS with decreasing rotor period, but increases in CPMG with decreasing π pulse spacing. Thus, the optimum echo

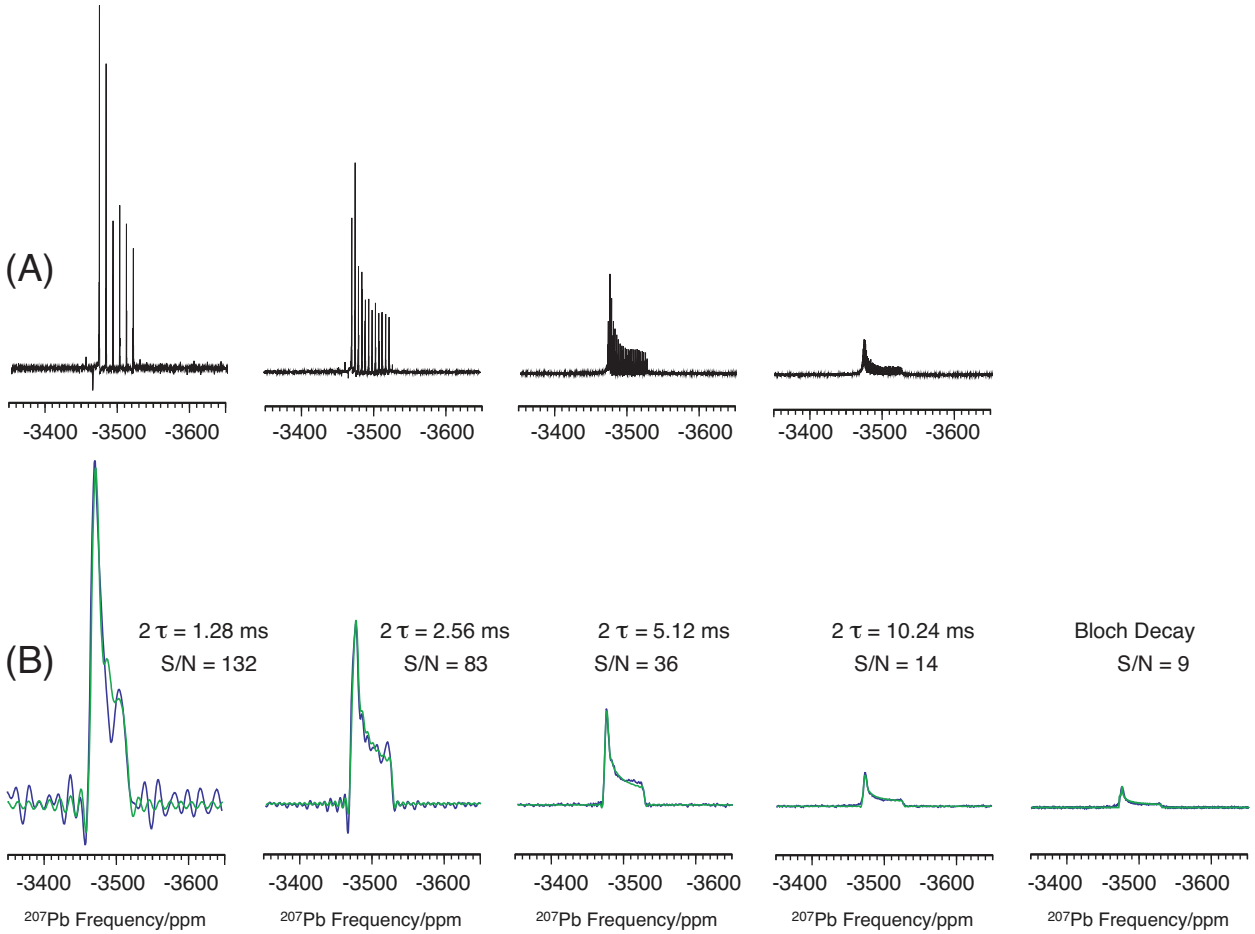

FIG. 4. The static CPMG experimental spectra of ^{207}Pb resonance in $Pb(NO_3)_2$ powder sample as function of π pulse spacing. (a) Processed using spikelet approach of Larsen *et al.* (Ref. 4). (b) Processed using modified TOP (Ref. 11) data processing method. Also shown are the best-fit model lineshapes which take signal truncation inside 2τ acquisition window into account.

cycle time for extracting the nuclear shielding tensor from a sideband analysis of MAS may not necessarily be the same for CPMG.

The tradeoff between spectral sensitivity and spectral content is well illustrated in Fig. 4 with a series of TOP-CPMG spectra of a ^{207}Pb anisotropic nuclear shielding lineshape in static $Pb(NO_3)_2$ measured as a function of CPMG π pulse spacing. As expected, with decreasing CPMG π pulse spacing the sensitivity of the spectrum increases by over an order of magnitude compared to the Bloch decay spectrum. For comparison, we also show the sideband (or spikelet) spectra obtained with a simple Fourier transform of the CPMG echo train. Note that the distortions due to signal truncation are more easily discernable in the TOP-CPMG spectra than the sideband spectra. As the CPMG π pulse spacing decreases, the spectrum becomes a convolution with a sinc function of increasing linewidth. When extracting the nuclear shielding tensor parameters, we can include the effect of this signal truncation in the shielding anisotropy lineshape model to improve the least-squares fit. Even with this improvement, however, the information about the shielding tensor is eventually lost as the π pulse spacing decreases and the sinc function lineshape dominates the spectrum. This loss of information about the shielding tensor is best reflected in the changing standard deviation of the principal components of the shielding tensor obtained in a least-squares analysis of the spectra as a function of CPMG π pulse spacing and shown in Table I. Compared to the Bloch decay, the uncertainty of extracted principal components decreases using CPMG with the minimum uncertainty obtained in the least-squares fit of the TOP-CPMG spectrum with 2τ=5.12 ms. More importantly, note that the principal component uncertainty gets progressively larger with further decrease in π pulse spacing, even though the sensitivity of the TOP-CPMG continues to increase with decreasing π pulse spacing. The values of δ_{11}, δ_{22}, and δ_{33} obtained from the lowest standard deviation fit correspond to

TABLE I. The principal components δ_{11}, δ_{22}, and δ_{33} of the chemical shift tensor and their associated errors obtained from a least-squares analysis of the ^{207}Pb TOP-CPMG spectra in Fig. 4 for a static sample of polycrystalline $Pb(NO_3)_2$ as a function of the CPMG π pulse spacing.

2τ (ms)	δ_{11} (ppm)	δ_{22} (ppm)	δ_{33} (ppm)	S/N
∞	$-3473.3 \pm \mathbf{0.05}$	$-3476.0 \pm \mathbf{0.05}$	$-3531.1 \pm \mathbf{0.17}$	9
10.24	$-3471.8 \pm \mathbf{0.05}$	$-3473.7 \pm \mathbf{0.04}$	$-3527.4 \pm \mathbf{0.16}$	14
5.12	$-3472.2 \pm \mathbf{0.02}$	$-3473.3 \pm \mathbf{0.02}$	$-3527.6 \pm \mathbf{0.07}$	36
2.56	$-3470.0 \pm \mathbf{0.04}$	$-3476.7 \pm \mathbf{0.04}$	$-3527.5 \pm \mathbf{0.10}$	83
1.28	$-3467.5 \pm \mathbf{0.17}$	$-3473.6 \pm \mathbf{0.17}$	$-3518.1 \pm \mathbf{0.21}$	132

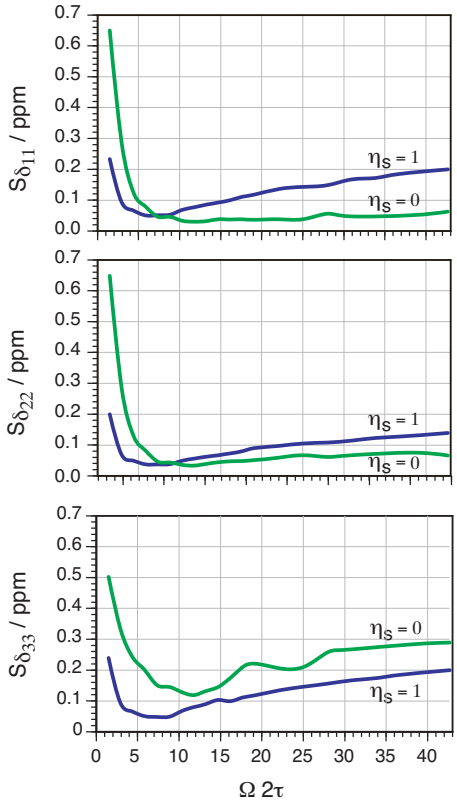

FIG. 5. Standard deviation of ^{207}Pb chemical shift tensor principal components (δ_{11}, δ_{22}, δ_{33}) extracted from simulated ^{207}Pb resonance CPMG spectra as a function of $\Omega\ 2\tau$ for different η while keeping span (Ω=4.58 kHz) and pre-CPMG signal to noise ratio (S/N=2.30) constant.

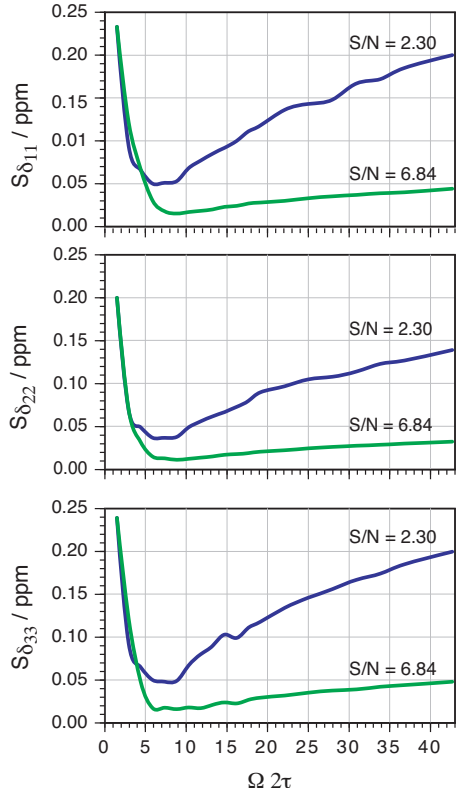

FIG. 6. Standard deviation of ^{207}Pb chemical shift tensor principal components (δ_{11}, δ_{22}, δ_{33}) extracted from simulated ^{207}Pb resonance CPMG spectra as a function of $\Omega\ 2\tau$ for different pre-CPMG signal-to-noise ratios while keeping span (Ω=4.58 kHz) and asymmetry parameter (η=1) constant.

ζ_s=−36.58 ppm and η_s=0.02, which are in close agreement with values of ζ_s=−36 ppm and η_s=0 reported by Neue *et al.*[15] Small differences in ζ_s and η_s may be attributed to the high sensitivity of the ^{207}Pb shielding tensor to temperature.[16]

For a more detailed understanding of how the shielding tensor parameter uncertainties depend on the CPMG π pulse spacing, we have simulated TOP-CPMG spectra using different π pulse spacing with constant total acquisition time, constant added noise (pre-CPMG S/N is 2.3), and a constant span of Ω=4.58 kHz. Least-squares analyses of simulated TOP-CPMG spectra were performed using a shielding lineshape model that takes the 2τ acquisition truncation into account. The standard deviations for the three principal components obtained in this analysis are plotted as a function of $\Omega\ 2\tau$ in Fig. 5 for η_s=0 and η_s=1 cases. The rise in uncertainty of the tensor parameters on the left side of the plots in Fig. 5 comes from the signal truncation inside the 2τ acquisition, window while the rise in uncertainty on the right side depends on the pre-CPMG signal-to-noise ratio (*vide infra*).

It is not surprising in the $\eta_s \approx 0$ case that the component δ_{33} is more susceptible to noise than δ_{11} and δ_{22} since it is associated with the lowest intensity singularity. For similar reasons both δ_{11} and δ_{33} in the η=1 case are more susceptible to noise than δ_{22}, as observed by their higher uncertainties in the high $\Omega\ 2\tau$ region. The minimum uncertainty occurs at different $\Omega\ 2\tau$ values for different η_s values, but appears to occur at the same $\Omega\ 2\tau$ for all three components of shielding tensor with a given η_s. All the standard deviation curves have a relatively shallow minimum, particularly for the δ_{22} component, which is always associated with the singularity of strongest intensity. When reporting the range of optimum $\Omega\ 2\tau$ values for a given lineshape, we report the $\Omega\ 2\tau$ value with minimum standard deviation and set the leftmost and rightmost limits as the $\Omega\ 2\tau$ value where the standard deviation reaches a value 50% higher than the minimum. Because of the asymmetry in the standard deviation curves, the range limits are not equidistant from the minimum $\Omega\ 2\tau$ value. Only the smallest range of the three tensor components will be reported. The minimum uncertainties in the η=0 case occur inside a range of $\Omega\ 2\tau \approx 12^{+6}_{-1}$, and in the case of η=1 inside a range of $\Omega\ 2\tau \approx 9^{+3}_{-3}$.

As noted, the lower bound of the optimum $\Omega\ 2\tau$ value arises from signal truncation and is fixed for a particular lineshape, independent of the pre-CPMG signal-to-noise ratio. Since the upper bound depends on the pre-CPMG signal-to-noise ratio, we have further investigated this dependence by simulating TOP-CPMG spectra with η_s=1 and Ω=4.58 kHz for two different pre-CPMG signal-to-noise ratios as shown in Fig. 6. As the pre-CPMG signal-to-noise ratio increases, the minima of the standard deviation curves become shallower, causing the upper bound for optimum range of $\Omega\ 2\tau$ values to increase. As seen in Fig. 6, increasing the pre-CPMG signal-to-noise ratio from 2.30 to 6.84 expands the range from $\Omega\ 2\tau \approx 9^{+3}_{-3}$ to $\Omega\ 2\tau \approx 9^{+7}_{-3}$. Clearly, further increases in the pre-CPMG sensitivity essentially eliminate the need for CPMG acquisition in reducing uncertainty in tensor parameter determinations. This is consistent

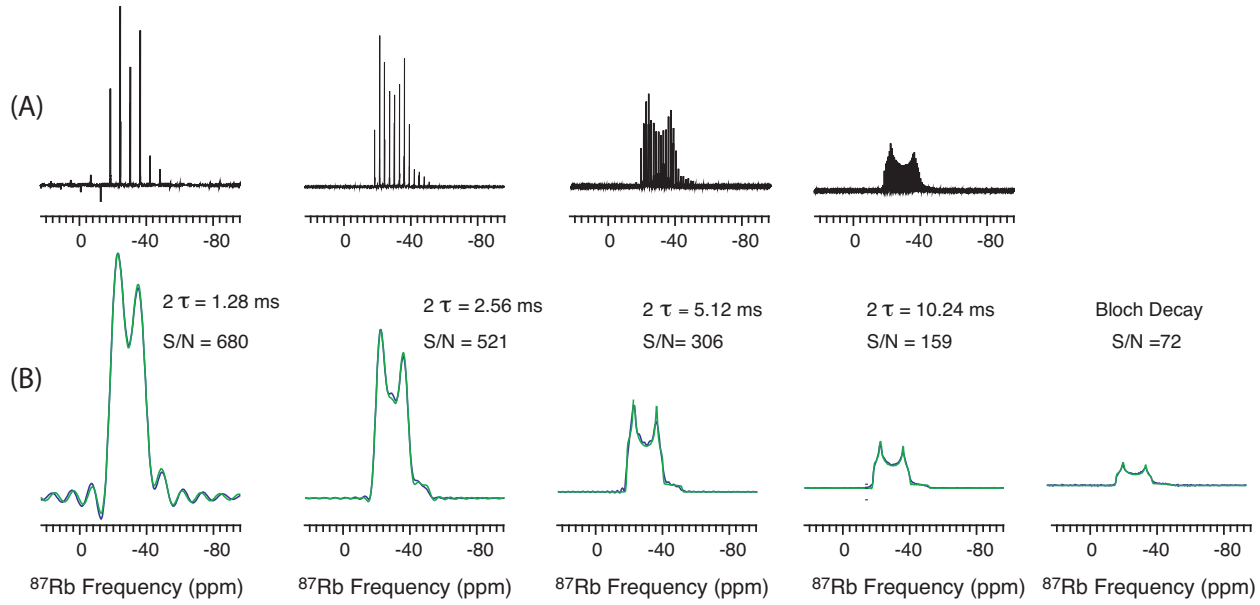

FIG. 7. The CPMG-MAS experimental spectra of ^{87}Rb resonance in $RbClO_4$ powder sample as a function of π pulse spacing, which was synchronized to the rotor period of 80 μs (ν_R=12.5 kHz). (a) CPMG data processed by spikelet approach of Larsen *et al.* (Ref. 4). (b) CPMG data processed by TOP (Ref. 11) approach. Also shown are the best-fit model lineshapes which take signal truncation inside 2τ acquisition window into account.

with conventional wisdom that the biggest gains with CPMG acquisition come when the pre-CPMG signal suffers from poor sensitivity. Conversely, as the sensitivity decreases the minima of the standard deviation curves become deeper and the range of optimum Ω 2τ values decreases. In the light of this insight, it may be worthwhile to extend the work of Hodgkinson and Emsley[8] to consider the effects of static sample signal sensitivity in determining the optimum range of MAS sidebands for extracting CSA tensor parameters.

B. Second-order quadrupolar coupling

The CT of half-integer spin nuclei is unaffected to first-order by the quadrupole coupling and for sizable quadrupole coupling constants experiences a second-order anisotropic frequency contribution that is not completely removed by MAS. The sensitivity of the CT spectrum of half-integer quadrupole nuclei under both static and MAS can be significantly enhanced with CPMG, so we have examined the optimum CPMG π pulse spacing for measuring both nuclear shielding and quadrupole coupling tensor parameters.

Since the nuclear shielding anisotropy is completely removed by fast MAS, the quadrupole coupling constant C_q and asymmetry parameter η_q can be readily determined from a least-squares analysis of the high speed CT MAS spectrum. These parameters, in turn, can be used as constraints in a least-squares analysis of the static sample CT spectrum to obtain the shielding tensor parameters and the relative orientation between the quadrupole and shielding tensors. In the case of $RbClO_4$, however, the ^{87}Rb quadrupole coupling constant is temperature dependent,[17,18] and frictional heating from the sample spinning is known[18] to reduce the value of ^{87}Rb quadrupole coupling constant in $RbClO_4$. Thus, without careful temperature control during MAS, systematic errors in the nuclear shielding tensor parameters could be introduced if the C_q and η_q values obtained from MAS fit were used to constrain the fit of the CT spectrum of a static $RbClO_4$ sample at room temperature.

Experimental TOP-CPMG-MAS CT spectra of ^{87}Rb resonance from polycrystalline $RbClO_4$ as a function of π pulse spacing are shown in Fig. 7. To avoid interference with the MAS averaging of anisotropies, it is important when combining CPMG with MAS that the π pulse spacing be synchronized to be an integer multiple of the rotor period. As expected, CPMG acquisition provides over an order of magnitude sensitivity enhancement compared to the Bloch decay experiment. Once again, notice that the lineshape distortions due to signal truncation are more easily discernible in the TOP-CPMG rather than the sideband spectrum. As before, we include the effect of this signal truncation in the second-order quadrupole MAS lineshape model to improve the least-squares fit. These "best fit" lineshapes are also shown in Fig. 7 for the TOP-CPMG spectra. The dependence of the uncertainty in C_q and η_q on the CPMG π pulse spacing is observed in their standard deviations shown in Table II. The CPMG π pulse spacing that gives the minimum uncertainty for C_q and η_q values is 2τ=2.56 ms, with values of 3.17

TABLE II. The quadrupole coupling parameters C_q and η_q and their associated errors obtained from a least-squares analysis of the ^{87}Rb TOP-CPMG MAS spectra in Fig. 7 for a polycrystalline sample of $RbClO_4$ as a function of the CPMG π pulse spacing.

2τ (ms)	C_q (MHz)	η_q	δ_{iso} (ppm)	S/N
∞	3.1542±**0.0022**	0.2086±**0.0013**	−12.802±**0.020**	72
10.24	3.1651±**0.0012**	0.2076±**0.0006**	−12.813±**0.010**	159
5.12	3.1694±**0.0009**	0.2065±**0.0006**	−12.809±**0.009**	306
2.56	3.1681±**0.0009**	0.2037±**0.0005**	−12.959±**0.008**	521
1.28	3.2075±**0.0026**	0.2816±**0.0016**	−11.553±**0.022**	680

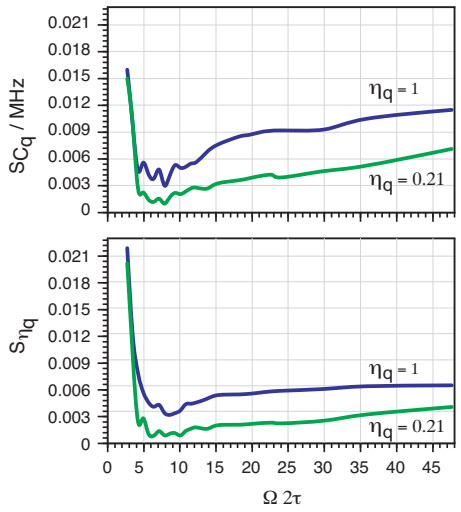

FIG. 8. The standard deviation of the ^{87}Rb quadrupolar coupling constant and asymmetry parameter extracted from simulated ^{207}Pb resonance CPMG-MAS spectra as a function of $\Omega\ 2\tau$ for η_q=0.21 and η_q=1, while keeping span ($\Omega_{q,\mathrm{MAS}}$=4.48 kHz) and pre-CPMG signal-to-noise ratio (S/N=6.93) constant. A spinning speed of 12.5 kHz was used for simulation.

MHz and 0.20, respectively. These values differ slightly from the values of C_q=3.3 MHz and η_q=0.21 obtained by Vosegaard *et al.*[20] in their single-crystal study. Given the previously mentioned temperature dependence of C_q in $RbClO_4$ this is not surprising. The ^{87}Rb MAS CT spectrum has a span of $\Omega_{q,\mathrm{MAS}}$=4,399 Hz, so the minimum uncertainty is obtained at $\Omega_{q,\mathrm{MAS}}2\tau \approx 11$ in this set of experiments.

To better understand how CPMG acquisition affects the uncertainty in C_q and η_q, we have simulated ^{87}Rb TOP-CPMG-MAS spectra as a function of CPMG π pulse spacing for two different asymmetry parameters, η_q=0.21 and η_q=1, while holding the span (Ω=4.48 kHz), pre-CPMG signal-to-noise ratio, and the total acquisition time constant. Plots of the standard deviations for C_q and η_q as a function of $\Omega\ 2\tau$ are shown in Fig. 8. The minimum uncertainties in both C_q and η_q occur in the range $\Omega\ 2\tau \approx 9^{+3}_{-2}$. There is a general increase in uncertainty for both C_q and η_q when η_q=1, which could be simply explained by the decrease in the number and intensity of discontinuities in the CT MAS lineshape when η_q=1.

Finally, we examined the CPMG acquisition for the ^{87}Rb CT spectra of a static polycrystalline sample of $RbClO_4$. The TOP-CPMG CT spectra as a function of 2τ are shown in Fig. 9. As before, lineshape distortions due to signal truncation are more easily discernible in the TOP-CPMG spectrum than the sideband spectrum. Using constraints of C_q=3.3 MHz and η_q=0.21 obtained from the single-crystal study,[20] and including the effects of signal truncation from the 2τ acquisition window, we performed a least-squares analysis of each lineshape and obtained the nuclear shielding tensor parameters, ζ_s, η_s, and their relative orientations, α, β, and γ, to the quadrupole tensor as a function of CPMG π pulse spacing. These values are shown in Table III. Although we have an expression in Eq. (10) for the span of a CT lineshape in a static sample due to second-order quadrupole interaction, we

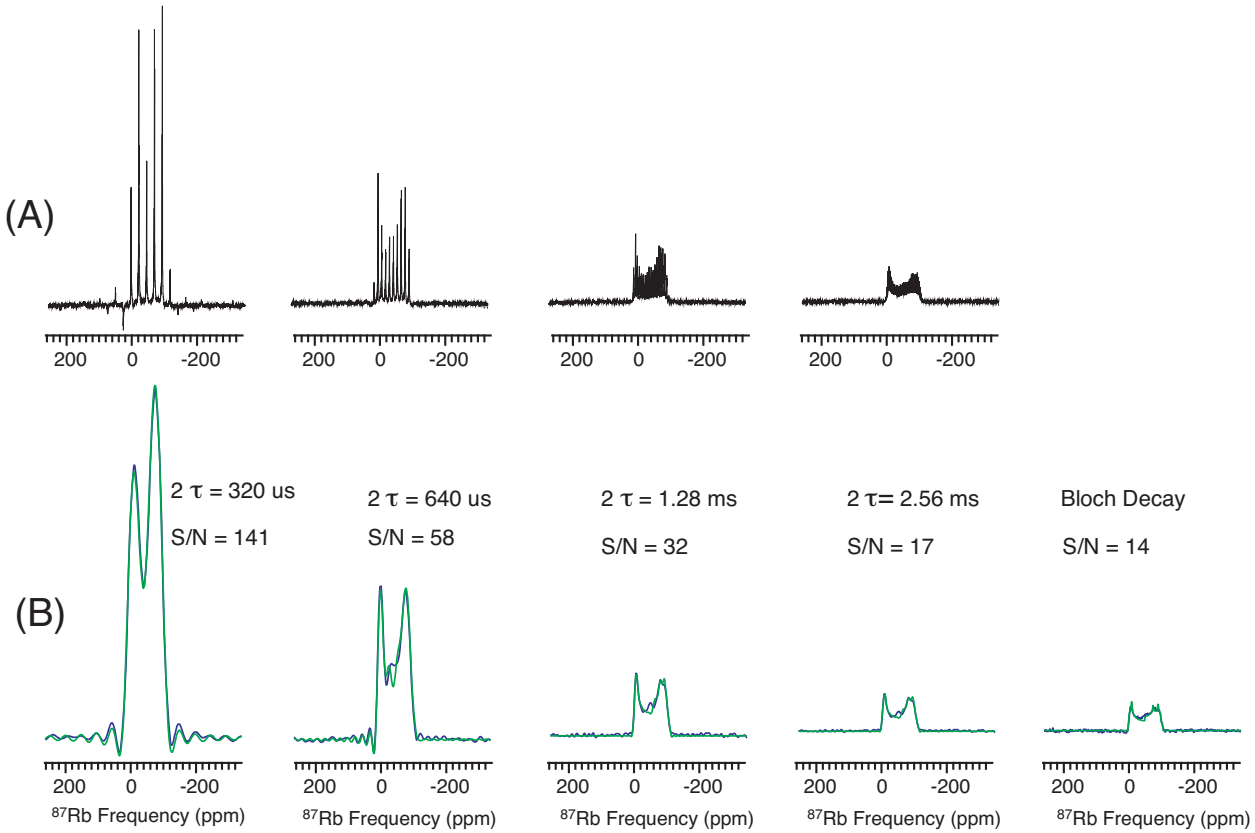

FIG. 9. The static CPMG experimental spectra of ^{87}Rb resonance in $RbClO_4$ powder sample as function of π pulse spacing. Top row is processed using spikelet approach of Larsen *et al.* (Ref. 4). The bottom row is processed using our modified TOP (Ref. 11) processing method. Also shown are the best-fit model lineshapes which take signal truncation inside 2τ acquisition window into account.

TABLE III. The ^{87}Rb nuclear shielding parameters ζ_s, η_s, and the Euler angles α, β, and γ describing the relative orientation of the nuclear shielding anisotropy tensor to the quadrupole tensor for ^{87}Rb and their associated errors obtained from a least-squares analysis of the ^{87}Rb TOP-CPMG spectra spectra in Fig. 9 for a static sample of polycrystalline $RbClO_4$ as a function of the CPMG π pulse spacing.

2τ (ms)	ζ_s (ppm)	η_s	α	β	γ	S/N
∞	$10.85 \pm \mathbf{0.26}$	$0.41 \pm \mathbf{0.01}$	$154.11° \pm \mathbf{4.01}°$	$33.68° \pm \mathbf{0.79}°$	$107.70° \pm \mathbf{2.91}°$	14
2.56	$12.33 \pm \mathbf{0.17}$	$0.49 \pm \mathbf{0.03}$	$153.53° \pm \mathbf{2.92}°$	$21.31° \pm \mathbf{0.59}°$	$77.35° \pm \mathbf{4.01}°$	17
1.28	$12.35 \pm \mathbf{0.19}$	$0.60 \pm \mathbf{0.02}$	$150.67° \pm \mathbf{2.86}°$	$16.61° \pm \mathbf{0.55}°$	$66.97° \pm \mathbf{3.95}°$	32
0.640	$13.18 \pm \mathbf{0.11}$	$0.66 \pm \mathbf{0.04}$	$123.76° \pm \mathbf{2.52}°$	$15.86° \pm \mathbf{0.51}°$	$100.16° \pm \mathbf{3.15}°$	58
0.320	$16.11 \pm \mathbf{0.41}$	$0.92 \pm \mathbf{0.07}$	$107.13° \pm \mathbf{5.15}°$	$27.49° \pm \mathbf{1.25}°$	$151.09° \pm \mathbf{4.79}°$	141

are not aware of an analytical expression that includes the effects of both quadrupole and nuclear shielding interactions. Nonetheless, Eq. (10) could provide an approximate span if an estimate of the quadrupolar coupling parameters is available. With the experimental span of $\Omega_{q,\mathrm{Static}}=18$ kHz and a minimum uncertainty found almost consistently at $2\tau=640$ μs for all parameters in the least-squares analysis of the static TOP-CPMG lineshapes, we experimentally observe that $\Omega_{q,\mathrm{Static}}2\tau=11.5$. A value consistent with the optimum range of values was observed for both the static nuclear shielding lineshape and the MAS CT second-order quadrupole lineshape.

Table IV is a comparison between the parameters obtained from our least-squares analysis of the TOP-CMPG spectrum and single-crystal study of Vosegaard *et al.*[20] The values of ζ_s and η_s are very similar to the reported value from single-crystal study, however, the values of α, β, and γ are not fully in agreement with the single-crystal study. This difference is simply attributed to the general ill-posed problem of fitting a CT spectrum of a static polycrystalline sample for both nuclear shielding and quadrupole coupling parameters and their relative tensor orientation. This challenge in analyzing CT anisotropic lineshapes in polycrystalline samples was the motivation behind the development of the two-dimensional COASTER (Ref. 21) experiment which cleanly separates the nuclear shielding and second-order quadrupole anisotropic lineshapes, thereby eliminating the covariance between nuclear shielding and quadrupole tensor components, and significantly reducing model parameter uncertainties.

V. SUMMARY

CPMG acquisition has become an increasingly popular approach for increasing sensitivity of solid-state NMR spectra that have significant inhomogeneous (i.e., anisotropic) broadenings. While increasing sensitivity is important, in the case of CPMG it comes with a loss of information about the NMR spin interactions. We have attempted to quantify this information loss in terms of the uncertainty of the NMR interaction tensor parameters extracted in a least-squares analysis of the CPMG-enhanced spectrum obtained as a function of CPMG π pulse spacing. To aid in this analysis we introduce the use of TOP processing for the CPMG signal echo train to obtain a more conventional powder pattern lineshape, instead of using a direct Fourier transform of the echo train signal which yields a sideband (or spikelet) spectrum. The TOP processed CPMG spectrum also has the advantage that the effect of signal truncation inside the 2τ CPMG acquisition window is readily discerned.

From our investigations of TOP-CPMG spectra with extensive least-squares analyses, we found for an anisotropic nuclear shielding or chemical shift lineshape in a static sample that the range of optimum π pulse spacings which minimize NMR parameter uncertainty while maximizing enhancement occur when $\Omega\ 2\tau \approx 12^{+6}_{-1}$ for $\eta_s=0$ and $\Omega\ 2\tau \approx 9^{+3}_{-3}$ for $\eta_s=1$, where 2τ is the π pulse spacing, Ω is the span of the anisotropic lineshape, and η_s is the asymmetry parameter for the nuclear shielding tensor. For an anisotropic second-order quadrupolar central transition lineshape under MAS a range of $\Omega\ 2\tau \approx 9^{+3}_{-2}$, regardless of η_q, minimized the uncertainty when determining the quadrupole tensor parameters.

Generally, the optimum π pulse spacing occurs in a range of values asymmetrically spaced around $\Omega\ 2\tau \sim 11$, regardless of the interactions contributing to the lineshape. The analyses and conclusions described here are applicable

TABLE IV. Comparison of previously measured ^{87}Rb nuclear shielding anisotropy (ζ_s, η_s) and the relative orientations (α, β, γ) of the nuclear shielding anisotropy tensor to the quadrupole tensor in $RbClO_4$. Values in this work were obtained for ^{87}Rb resonance in $RbClO_4$ powder by fitting the static CPMG spectra with the quadrupole coupling principal components constrained to $C_q=3.3$ MHz and $\eta_q=0.21$. The definition of (α,β,γ) is in accord with the definition used in Ref. 19.

Method	ζ_s (ppm)	η_s	α	β	γ	Reference
Static powder	$13.18 \pm \mathbf{0.11}$	$0.66 \pm \mathbf{0.04}$	$123.76° \pm \mathbf{2.52}°$	$15.86° \pm \mathbf{0.51}°$	$100.16° \pm \mathbf{3.15}°$	This work
Single-crystal	$13.80 \pm \mathbf{1.50}$	$0.61 \pm \mathbf{0.24}$	$94.00° \pm \mathbf{14.0}°$	$28.00° \pm \mathbf{4.00}°$	$87.00° \pm \mathbf{5.00}°$	18
Static powder	$14 \pm \mathbf{2}$	$0.5 \pm \mathbf{0.3}$	$112.00° \pm \mathbf{6.0}°$	$28.80° \pm \mathbf{1.5}°$	$16.00° \pm \mathbf{4.00}°$	19

to any CMPG-enhanced solid-state NMR experiment and thus should serve to reduce significantly experimental setup and optimization times.

ACKNOWLEDGMENTS

We acknowledge helpful discussions with Professor Robert Schurko and financial support from National Science Foundation under Grant No. CHE-0616881.

APPENDIX A: PERIODIC SIGNALS AND SIDEBANDS

In this section we will consider the relationship between a periodic signal and the sideband pattern in its Fourier transform. First, we write a Fourier series expansion of the periodic signal according to

$$S_T(t) = \sum_{N=-\infty}^{\infty} A(N) e^{i2\pi Nt/T}, \tag{A1}$$

whose Fourier transform is

$$S_T(\omega) = \int_{-\infty}^{\infty} S_T(t) e^{-i\omega t} dt = \sum_{N=-\infty}^{\infty} A(N)\delta(2\pi N/T - \omega), \tag{A2}$$

where T is the signal period and $A(N)$ is the amplitude of the Nth sideband in $S_T(\omega)$.

Next, we define $S_T(t)$ as a periodic extension of a signal, $S(t)$, defined only inside a period from $t=0$ to T, according to

$$S_T(t) = \sum_{n=-\infty}^{\infty} S(t+nT), \tag{A3}$$

whose Fourier transform is

$$S_T(\omega) = \int_{-\infty}^{\infty} \left[\sum_{n=-\infty}^{\infty} S(t+nT) \right] e^{-i\omega t} dt. \tag{A4}$$

Performing a change in variables, defining $s=t+nT$, and $ds=dt$, we obtain

$$S_T(\omega) = \sum_{n=-\infty}^{\infty} \int_{-\infty}^{\infty} S(s) e^{-i\omega(s-nT)} ds. \tag{A5}$$

Since $S(t)$ is defined only inside a period from $t=0$ to T, we can redefine the integral limits, obtaining

$$S_T(\omega) = \sum_{n=-\infty}^{\infty} \left[\int_0^T S(s) e^{-i\omega s} ds \right] e^{in\omega T}. \tag{A6}$$

Equating the two expressions for the Fourier transform of $S_T(t)$,

$$A(N)\delta(2\pi N/T - \omega) = \left[\int_0^T S(s) e^{-i\omega s} ds \right] e^{in\omega T}, \tag{A7}$$

we obtain

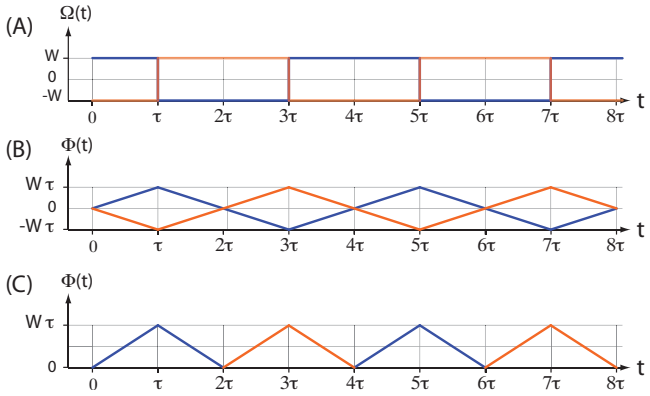

FIG. 10. (a) Time dependent frequency and (b) time dependent phase for the two pathway signals in the CPMG experiment. (c) The time dependent phase of the detected CPMG signal.

$$A(N) = \int_0^T S(s) e^{-i2\pi Ns/T} ds, \tag{A8}$$

as the relationship between the Nth sideband in $S_T(\omega)$ and the signal $S(t)$ defined inside the period from $t=0$ to T.

APPENDIX B: CPMG SIGNAL

The CPMG signal arises from the two coherence transfer pathways shown in Fig. 1. Signal from a given pathway is detected only while its coherence level is $p=-1$. Both pathway signals experience a time dependent frequency with a period of 4τ, where 2τ is the CPMG π pulse spacing. As shown in Fig. 10(a), we can describe the time dependent frequencies for the two pathway signals as

$$\Omega_{\pm}(t) = \pm W(\alpha,\beta,\gamma)\mathrm{Sq}(2\pi t/4\tau), \tag{B1}$$

where $\mathrm{Sq}(x)$ is a square wave function and 4τ is the cycle time of the frequency for the two pathway signals. As the integral of a square wave is a triangular wave, the signal phases for the two pathways, shown in Fig. 10(b), are given by

$$\Phi_{\pm}(t) = \pm W(\alpha,\beta,\gamma)\tau\,\mathrm{Tg}(2\pi t/4\tau), \tag{B2}$$

where $\mathrm{Tg}(x)$ is a triangle wave function. A CPMG echo occurs whenever the signal phase returns to zero. Since the signals from the two pathways are detected alternatively, the detected signal phase, shown in Fig. 10(c), is given by

$$\Phi(t) = W(\alpha,\beta,\gamma)\tau\left[\mathrm{Tg}\left(\frac{2\pi t}{2\tau} - \pi \right) + 1 \right], \tag{B3}$$

which has a period of $T=2\tau$. Thus, the detected CPMG signal inside the $0-2\tau$ period is given by

$$S(t) = e^{-iW(\alpha,\beta,\gamma)(\tau-|t-\tau|)}. \tag{B4}$$

[1] H. Y. Carr and E. M. Purcell, Phys. Rev. **94**, 630 (1954).
[2] S. Meiboom and D. Gill, Rev. Sci. Instrum. **29**, 688 (1958).
[3] E. L. Hahn, Phys. Rev. **80**, 580 (1950).
[4] F. H. Larsen, H. J. Jakobsen, P. D. Ellis, and N. C. Nielsen, J. Phys. Chem. A **101**, 8597 (1997).
[5] F. H. Larsen, H. J. Jakobsen, P. D. Ellis, and N. C. Nielsen, J. Magn. Reson. **131**, 144 (1998).
[6] F. H. Larsen, J. Skibsted, H. J. Jakobsen, and N. C. Nielsen, J. Am.

Chem. Soc. **122**, 7080 (2000).
[7] R. Lefort, J. W. Wiench, M. Pruski, and J. P. Amoureux, J. Chem. Phys. **116**, 2493 (2002).
[8] P. Hodgkinson and L. Emsley, J. Chem. Phys. **107**, 4808 (1997).
[9] P. Blumler, B. Blümich, and J. Jansen, Solid State Nucl. Magn. Reson. **3**, 237 (1994).
[10] B. Blümich, P. Blumler, and J. Jansen, Solid State Nucl. Magn. Reson. **1**, 111 (1992).
[11] D. Massiot, J. Hiet, N. Pellerin, F. Fayon, M. Deschamps, S. Steuernagel, and P. J. Grandinetti, J. Magn. Reson. **181**, 310 (2006).
[12] R. K. Harris, E. D. Becker, S. M. Cabral De Menezes, and R. E. Pierre Grangerd, Inorg. Chem. **3**, 41 (2008).
[13] D. Freude and J. Haase, NMR Basic Principle and Progress **21**, 1 (1993).
[14] R. R. Ernst, G. Bodenhausen, and A. Wokaun, *Principles of Nuclear Magnetic Resonance in One and Two Dimensions* (Oxford, Oxford, 1987).
[15] G. Neue, C. Dybowski, M. L. Smith, M. A. Hepp, and D. L. Perry, Solid State Nucl. Magn. Reson. **6**, 241 (1996).
[16] O. Dmitrenko, S. Bai, P. A. Beckmann, S. V. Bramer, A. J. Vega, and C. Dybowski, J. Phys. Chem. A **112**, 3046 (2008).
[17] J. Skibsted and H. J. Jakobsen, J. Phys. Chem. A **103**, 7958 (1999).
[18] T. Vosegaard, J. Skibsted, H. Bildsoe, and H. J. Jakobsen, J. Phys. Chem. **99**, 10731 (1995).
[19] J. M. Koons, E. Hughes, H. M. Cho, and P. D. Ellis, J. Magn. Reson. A **114**, 12 (1995).
[20] T. Vosegaard, J. Skibsted, H. Bildsoe, and H. J. Jakobsen, J. Magn. Reson. **122**, 111 (1996).
[21] J. T. Ash, N. T. Trease, and P. J. Grandinetti, J. Am. Chem. Soc. **130**, 10858 (2008).